

ONLY FROM TI	GET PIQUA™ TECHNOLOGY TI's System of IP Quality Management	TEXAS INSTRUMENTS Technology for Innovators™
-----------------	---	---

## CommsDesign

### Tutorial on PLLs: Part 1

James A. Crawford, Silicon RF Systems

" 05, 2004 (12:00 ♂H)

URL: <http://www.commsdesign.com/showArticle.jhtml?articleID=19502344>

Few topics in electrical engineering have demanded as much attention over the years as the phase-locked loop (PLL). The PLL is arguably one of the most important building blocks necessary for modern digital communications, whether in the RF radio portion of the hardware where it is used to synthesize pristine carrier signals, or in the baseband digital signal processing (DSP) where it is often used for carrier- and time-recovery processing. The PLL topic is also intriguing because a thorough understanding of the concept embraces ingredients from many disciplines including RF design, digital design, continuous and discrete-time control systems, estimation theory and communication theory.

The PLL landscape is naturally divided into (i) low signal-to-noise ratio (SNR) applications like Costas carrier-recovery and time-recovery applications and (ii) high SNR applications like frequency synthesis. Each of these areas is further divided between (a) analog/RF continuous-time implementations versus (b) digital discrete-time implementations. The different manifestations of the PLL concept require careful attention to different usage, analysis, design and implementation considerations.

With so many good tutorials about PLLs available on the Internet and elsewhere today, a theoretically unifying development will be presented in this article with the intention of providing a deepened understanding for this extremely pervasive concept. In Part 1 of this series we'll look at PLL basics as well as different perspectives on PLL theory. In [Part 2](#), we'll continue our look into PLL theory and then provide some real-world PLL design examples.

#### PLL Basics

The best way to develop a sound understanding of the PLL is to review the fundamental theories upon which this concept is based. One of the factors contributing to the longevity of the PLL is that relatively simple implementations can still lead to nearly optimal solutions and performance.

"While recovering from an illness in 1665, Dutch astronomer and physicist Christiaan Huygens noticed something very odd. Two of the large pendulum clocks in his room were beating in unison, and would return to this synchronized pattern regardless of how they were started, stopped or otherwise disturbed.

An inventor who had patented the pendulum clock only eight years earlier, Huygens was understandably intrigued. He set out to investigate this phenomenon, and the records of his experiments were preserved in a letter to his father. Written in Latin, the letter provides what is believed to be the first recorded example of the synchronized oscillator, a physical phenomena that has become increasingly important to physicists and engineers in modern times." (See [http://www.globaltechnoscan.com/20thSep-26thSep/out\\_of\\_time.htm](http://www.globaltechnoscan.com/20thSep-26thSep/out_of_time.htm))

It should come as no surprise that modern researchers would later find that the behavior of such injection-locked oscillators can be closely modeled based upon PLL principles.<sup>6,7,8,9</sup> Anyone who has tried to co-locate RF oscillators running at different but nearly the same frequency has experienced how incredibly sensitive this coupling phenomenon is!

In 1840, Alexander Bain proposed a fax machine that used synchronized pendulums to scan an image at the transmitting end and send electrical impulses to a matching pendulum at the receiving end to reconstruct the image. The device, however, was never developed.

"The phase-lock concept as we know it today was originally described in a published work by de Bellescize in 1932<sup>1</sup> but did not fall into widespread use until the era of television where it was used to synchronize horizontal and vertical video scans. One of the earliest patents showing the use of a PLL with a feedback divider for frequency synthesis appeared in 1970.<sup>2</sup> The PLL concept is now used almost universally in many products ranging from citizens band radio to deep-space coherent receivers."<sup>1</sup>

A PLL consists of three basic components that appear in one form or another:<sup>4,5</sup>

1. Phase error metric or detector
2. Frequency-controllable oscillator
3. Loop filter

Loop "type" refers to the number of ideal poles (or integrators) within the linear system. A voltage-controlled oscillator (VCO) is an ideal integrator of phase for example.

Loop "order" refers to the polynomial order of the describing characteristic equation for the linear system. Loop-order must always be greater than or equal to the loop-type.

Although the term "settling time" is frequently used in the literature, a specified settling time is meaningless unless the definition for settling is also provided. A properly rigorous statement would be for example, "The settling time for the PLL is 1.5 ms to within +/-5 degrees of steady-state phase."

### Continuous-Time Versus Discrete-Time Systems

PLL work was originally based upon continuous-time dynamics and engineers utilized the Laplace transform to mathematically describe linear PLL behavior. The world has however gone digital and with it, time has been discretized and dynamic quantities sampled. The connection between continuous-time and discrete-time systems can be easily bridged by making use of the Poisson Sum formula.<sup>3</sup> This formula relates the continuous-time function  $h(t)$  and its Fourier transform  $H(f)$  to the discretized world as:

$$\sum_k T_s h(kT_s) \exp(-j2\pi f k T_s) = \sum_m H\left(f \pm \frac{m}{T_s}\right) \quad (\text{Eq. 1})$$

where  $T_s$  is the time interval between samples. The left-hand side of Equation 1 is by definition the z-transform of  $h(t)$  weighted by the quantity  $T_s$ .

It is insightful to look at this statement for the classic type-2 third-order PLL shown in **Figure 1** for which the open-loop gain is given by:

$$G_{OL}(s) = \left(\frac{\omega_n}{s}\right)^2 \frac{1+s\tau_2}{1+s\tau_p} \quad (\text{Eq. 2})$$

$$\omega_n = \sqrt{\frac{K_d K_v}{N(C_1 + C_2)}} \quad (\text{Eq. 3})$$

$$\zeta = \frac{1}{2} \omega_n \tau_2 \quad (\text{Eq. 4})$$

$$\tau_2 = R_2 C_2 \quad (\text{Eq. 5})$$

$$\tau_p = \frac{C_1 C_2 R_2}{C_1 + C_2} \quad (\text{Eq. 6})$$

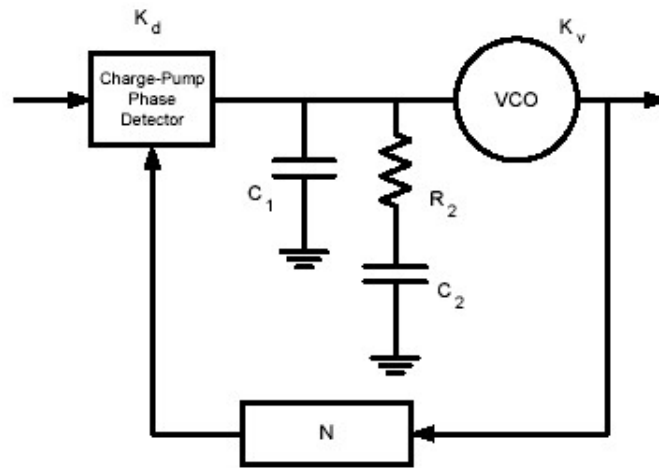


Figure 1: Diagram of a simple charge-pump PLL.

where  $K_V$  is the VCO tuning sensitivity (rad/sec/V),  $K_D$  is the phase detector gain (A/rad.),  $N$  is the feedback divider ratio, and  $\tau_p$  and  $\tau_2$  are the time constants associated with the lead-lag loop filter. In this form, the loop natural frequency and loop damping factor are given respectively by Equations 3 and 4.

The discrete-equivalent z-transform for  $G_{OL}(s)$  can be computed as:

$$G_{OL}(z) = \omega_n^2 Z \left[ \frac{1 + s\tau_2}{s^2(1 + s\tau_p)} \right] = \omega_n^2 \left[ \frac{(\tau_2 - \tau_p)z}{z-1} + \frac{zT_s}{(z-1)^2} + \frac{(\tau_p - \tau_2)z}{z - \exp\left(-\frac{T_s}{\tau_p}\right)} \right] \quad (\text{Eq. 7})$$

As developed at length in Chapters 4 and 5 of Reference 3, sampling control system factors adversely affect PLL stability, settling time, and phase noise performance as the closed-loop bandwidth is permitted to exceed approximately 1/10th of the phase comparison frequency. Sampling effects on the open-loop and closed-loop transfer functions can be assessed by either going to the trouble to first compute the z-transform of the open-loop gain function as in Equation 7, or the Poisson Sum formula can be used to compute the closed-loop transfer function much more conveniently as:

$$H(s) = \frac{G_{OL}(s)}{1 + \frac{1}{T_s} \sum_k G_{OL}\left(s + j\frac{2\pi k}{T_s}\right)} \quad (\text{Eq. 8})$$

Only a very few of the aliased  $G_{OL}(s)$  gain terms need to be retained in the denominator in order to very accurately capture the sampling effects of interest.

The open-loop gain functions with and without the inclusion of sampling effects are shown in **Figure 2** assuming a sampling rate of 100 kHz, a natural frequency of 5 kHz and damping factor of 0.90. The closed-loop response for this same system is shown in **Figure 3** using Equation 8.

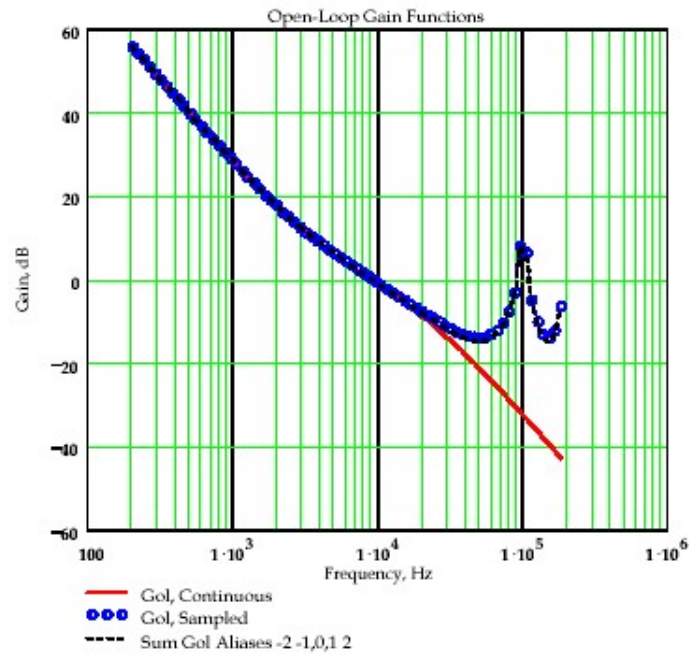


Figure 2: Closed-loop gain showing continuous and sampled gain forms.

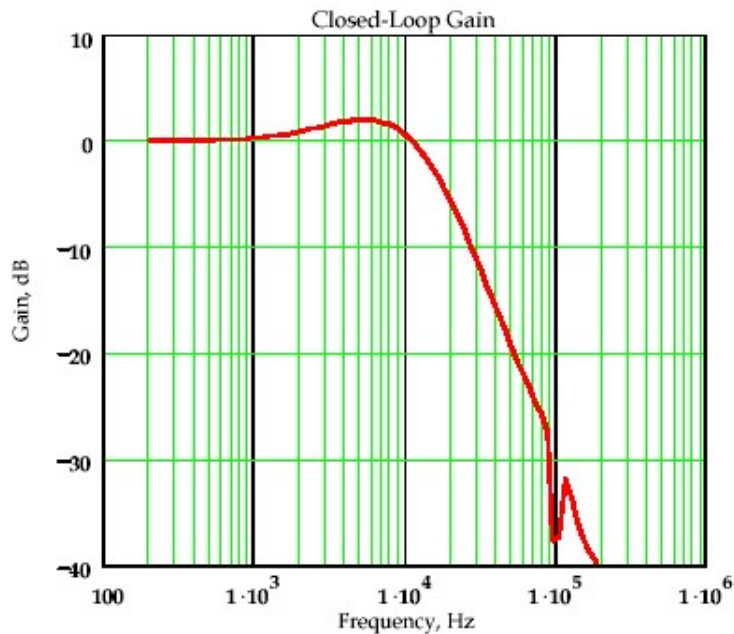


Figure 3: Closed-loop behavior for the case shown in Figure 2.

If the PLL natural frequency is increased to 12.5 kHz (representing 1/8th of the sampling rate), stability problems become readily apparent as an excessive amount of gain-peaking that appears as shown in **Figure 4** and the almost nonexistent gain-margin as shown in **Figure 5**.

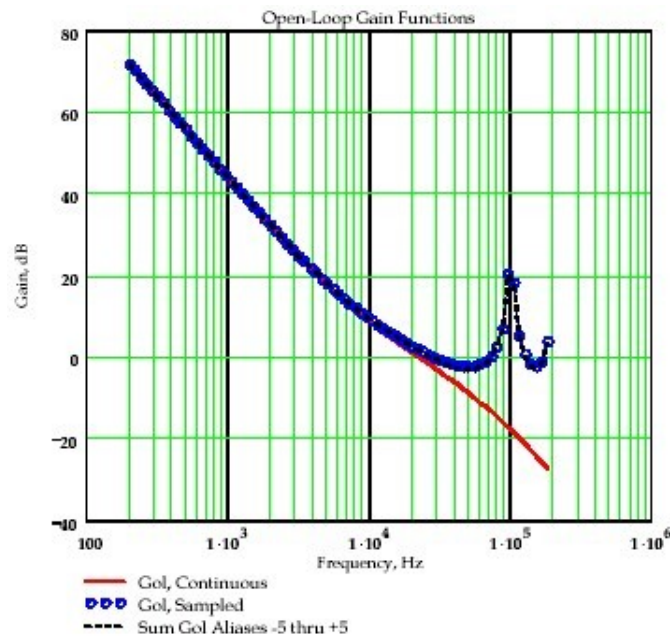


Figure 4: Open-loop gain for increased PLL bandwidth case.

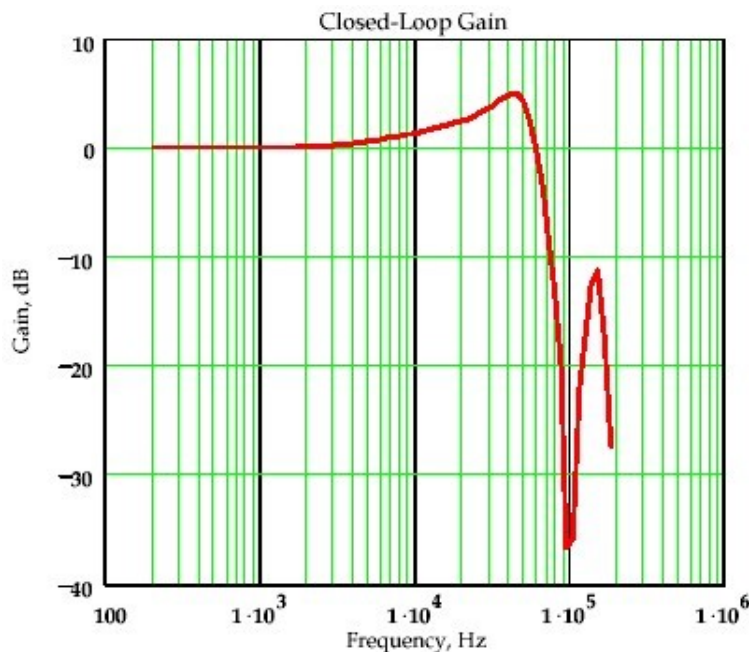


Figure 5: Closed-loop behavior for increased PLL bandwidth case.

### PLL Theory Perspectives

PLL theory of operation can be looked at from several different perspectives. As we have just seen in the previous section, time-continuous and sampled system analysis of PLLs used for frequency synthesis produce almost identical results unless the closed-loop bandwidth becomes an appreciable fraction of the phase comparison frequency being used.

In a similar fashion, different analysis must be used to study PLL operation under low signal-to-noise ratio (SNR) cases (e.g., customarily found in receiver applications) as compared to high SNR cases (e.g., like those encountered in frequency synthesizer usage). Several different perspectives that all help expand the phase-locked loop concept are discussed in the material that follows.

### Control Theory Perspective (High SNR)

The control theory perspective of PLLs is normally the setting with which electrical engineers are dominantly familiar. Control theory concepts were used earlier in this article. Continuing in this vein, the classical type-2 second-order PLL that will be used for these discussions is shown in **Figure 6**. In our first view of this PLL in the strictly continuous-time domain, the phase detector is assumed to be linear (i.e., no sample-and-hold present).

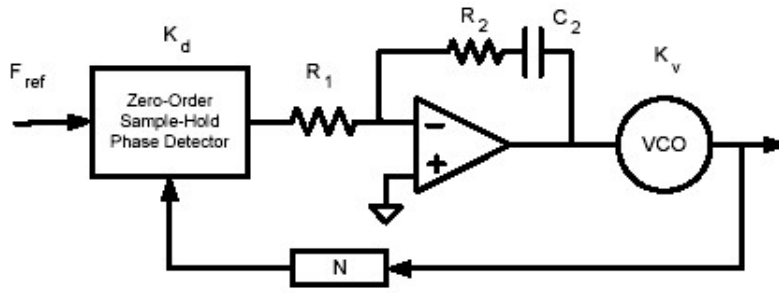


Figure 6: Classical type-2 second-order PLL with sample-and-hold phase detector.

$$\omega_n = \sqrt{\frac{K_d K_v}{N \tau_1}} \quad (Eq.9)$$

$$\zeta = \frac{1}{2} \omega_n \tau_2 \quad (Eq.10)$$

$$\omega_u = \omega_n \sqrt{2\zeta^2 + \sqrt{4\zeta^4 + 1}} \quad (Eq.11)$$

Several first-order approximations are helpful to keep in mind when dealing with this classical PLL system based upon simple Bode diagramming techniques. The open-loop gain diagram of interest is **Figure 7** whereas **Figure 8** pertains to the closed-loop characteristics. In both figures, the unity-gain radian frequency  $\omega_u$  is given by Equation 11.

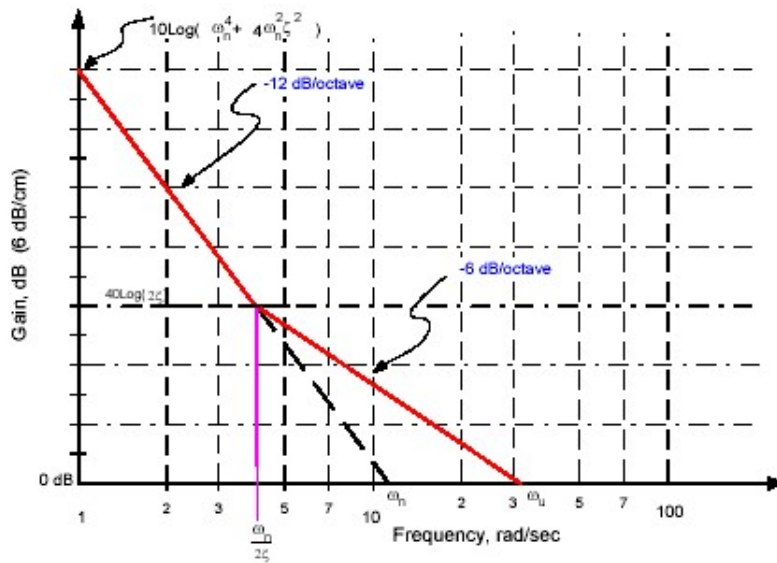


Figure 7: Open-loop gain approximations for classic type-2 PLL.

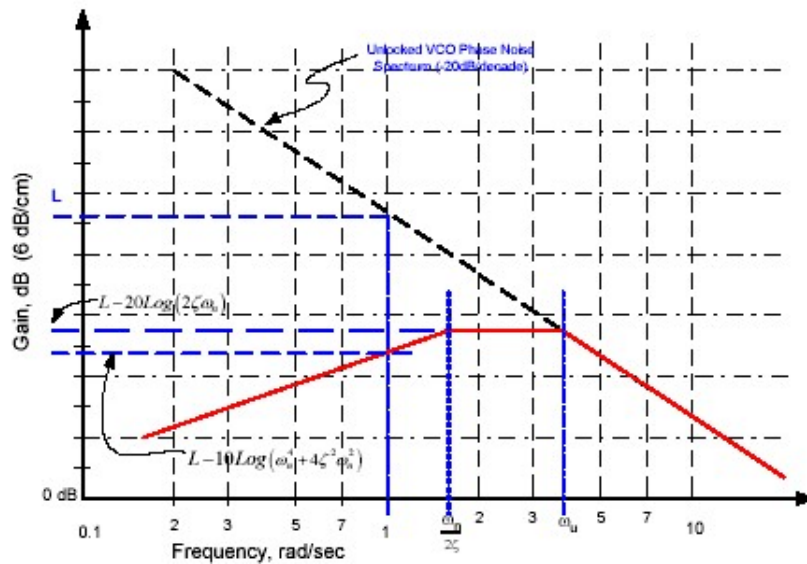


Figure 8: Closed-loop approximations for classic type-2 PLL.

As noted elsewhere, the behavior of real-world sampled systems matches the continuous-time behavior very closely if the system bandwidths are small relative to the sampling rate. Therefore, it is very convenient to use the results from continuous-time theory to approximate useful quantities for both types of systems. A number of these helpful results for the continuous-time case are provided in **Table 1**.

**Table 1 Helpful Formula for Classic Type-2 PLL**

[Click Here for Table 1](#)

In moving beyond the strictly continuous-time domain so that we can include digital dividers and phase detectors, we now include the zero-order sample-and-hold in the open-loop gain formula as given by Equation 12. In this formulation,  $K_d$  now has dimensions of V/rad. and  $T_s$  is the time between sampling instants. The closed-loop natural frequency and damping factor are still given by Equations 9 and 10 respectively.

$$\begin{aligned} G_{OL}(s) &= \frac{1}{T_s} \left( \frac{1 - e^{-sT_s}}{s} \right) \frac{K_d K_v}{N \tau_1} \frac{1 + s\tau_2}{s^2} \\ &= \frac{1}{T_s} \left( \frac{1 - e^{-sT_s}}{s} \right) \left( \frac{\omega_n}{s} \right)^2 \left( 1 + 2\zeta \frac{s}{\omega_n} \right) \quad (\text{Eq. 12}) \end{aligned}$$

In the case where the continuous-time open-loop gain is given by Equation 12, full sampling effects can be included by computing the equivalent z-transform for this open-loop gain function which is:

$$G_{OL}(z) = (\omega_n T_s)^2 \frac{z \left( \frac{1 + \tau_2}{2} + \frac{\tau_2}{T_s} \right) + \left( \frac{1 - \tau_2}{2} - \frac{\tau_2}{T_s} \right)}{(z-1)^2} \quad (\text{Eq. 13})$$

The system gain-margin  $G_M$  based upon Equation 13 can be shown to be:

$$G_M = -20 \text{Log}(\zeta \omega_n T_s) \quad (\text{Eq. 14})$$

But the gain margin is only defined provided that  $\omega_n T_s < 4\zeta$ . This same constraint applies for the system phase margin, which is given Reference 3. Since the z-domain shown in Equation 13 includes sampling effects whereas the Laplace s-domain in shown in Equation 12 does not, the gain-margin predicted using the Laplace transform  $G_{OL}(s)$  will always be more optimistic than actual as shown in **Figure 9**.

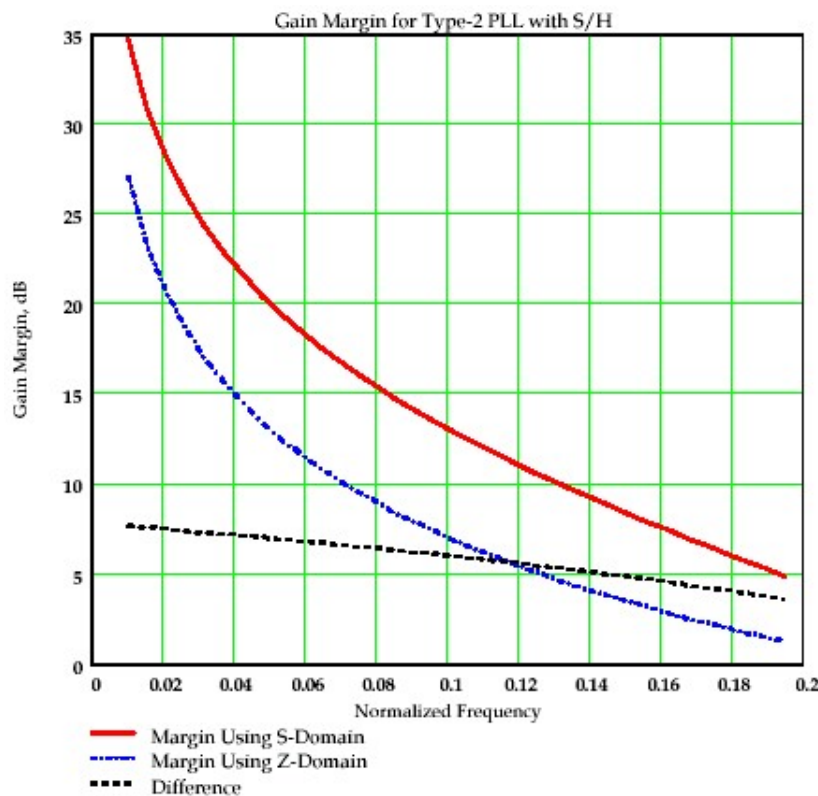


Figure 9: Gain margin for classic type-2 PLL with sample-and-hold  $\zeta=0.707$ .

### Phase-Locked Loops for Low SNR Applications

Low SNR applications are frequently observed at the receiving end of the system. The low SNR case can be cast in its most simple form as a simple sinusoidal signal immersed in additive white Gaussian noise (AWGN) and mathematically represented as:

$$r(t) = s(t) + n(t) \quad (\text{Eq. 15})$$

where  $s(t) = A \cos(\omega_0 t + \theta)$  and the frequency and phase are considered constant. In the phase-lock condition, we can further assume that the frequency  $\omega_0$  is known whereas the system is attempting to track the phase  $\theta$ , which is assumed to be quasi-static relative to the bandwidth of the PLL tracking system. It can be shown that the probability density function for the  $\theta$  estimate can be written as:

$$p(\theta, \gamma) = \frac{\exp(-\gamma^2)}{2\pi} \left\{ 1 + \gamma \sqrt{\pi} \cos(\theta) \exp[\gamma^2 \cos^2(\theta)] [1 + \text{erf}(\gamma \cos(\theta))] \right\} \quad (\text{Eq. 16})$$

where  $\gamma$  is the receive SNR. The cumulative pdf using Equation can be numerically computed to create the traditional "S-curve" for the ideal phase error metric. Example probability density functions and their associated S-curves are shown in **Figures 10** and **11**.



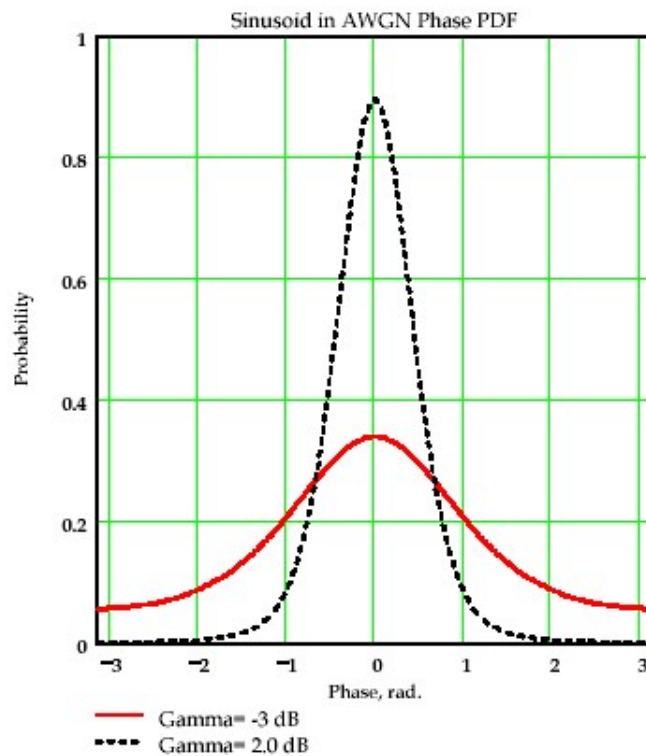


Figure 10: Phase error PDF.

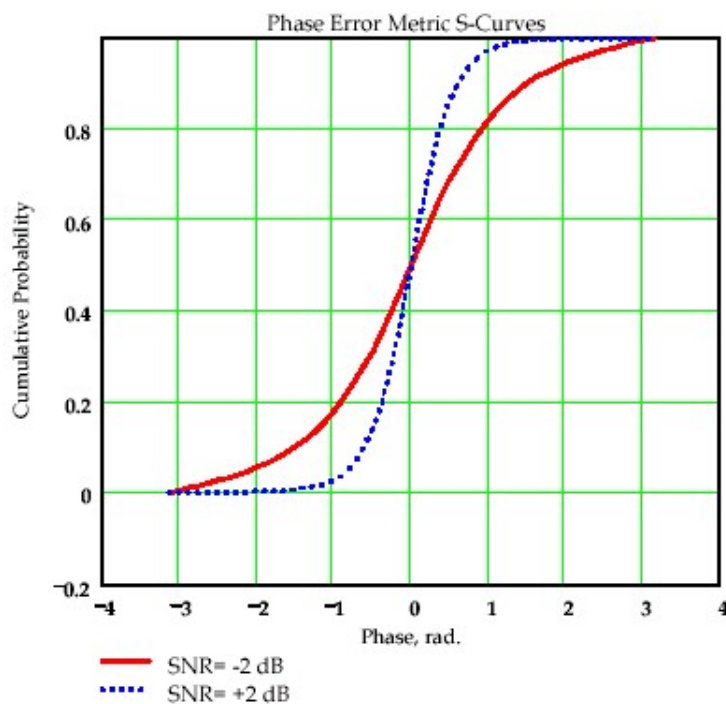


Figure 11: Cumulative phase error PDFs (S-curves).

Fokker-Planck techniques can be used to solve the ensuing closed-loop tracking performance question for type-1 PLLs.<sup>10,11,12</sup> The classic result that follows is the well-known Tikhonov probability density function for the closed-loop phase error given as:

$$P(\phi) = \frac{\exp[\rho \cos(\phi)]}{2\pi I_0(\rho)} \quad (\text{Eq. 17})$$

where  $\rho$  is the SNR within the closed-loop bandwidth and  $I_0(\cdot)$  is the modified Bessel function of order zero. A more insightful exploration into the tracking performance of the type-1 PLL can be made by using the S-curve results that were just presented along with a first-order Markov model for the

system.

In the first-order Markov model for a type-1 PLL<sup>13,14</sup>, the phase error range  $(-\pi, +\pi]$  is quantized across  $N$  states. Particularly nice closed-form results occur<sup>14</sup> if the state transitions are limited to strictly nearest-neighbor transitions as shown in **Figure 12**. Since the use of  $N$  states divides the total phase range of  $2\pi$  into  $N$  equally-spaced phase intervals, the closed-loop bandwidth is inversely proportional to  $N$ . The state-transition probabilities denoted by the  $p_i$  and  $q_i$  are directly obtained from the S-curve at the SNR of interest.

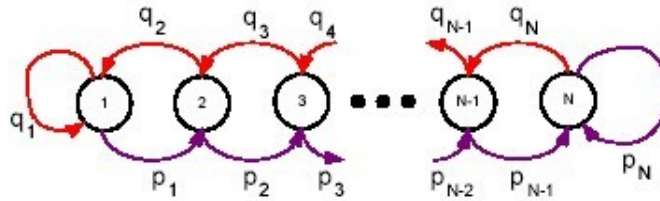


Figure 12: First-order Markov chain model for type-1 PLL.

The Markov steady-state probability equations can be formulated as:

$$S_1 = q_1 S_1 + q_2 S_2$$

$$S_N = p_N S_N + p_{N-1} S_{N-1} \quad (\text{Eq. 19})$$

$$S_k = p_{k-1} S_{k-1} + q_{k+1} S_{k+1} \quad (\text{Eq. 20})$$

in which the  $S_k$  denote the steady-state occupancy probabilities for each state with  $k=1\dots N$ . This set of equations can be solved as:

$$S_1 = \left\{ 1 + \sum_{k=2}^N \left[ \prod_{i=1}^{k-1} \frac{p_i}{q_{i+1}} \right] \right\}^{-1} \quad (\text{Eq. 21})$$

$$S_k = S_1 \prod_{i=1}^{k-1} \left( \frac{p_i}{q_{i+1}} \right) \text{ for } k=2 \text{ to } N \quad (\text{Eq. 22})$$

The mean tracking point and tracking error variance can be directly computed from the steady-state probabilities as:

$$\mu = \sum_{i=1}^N i S_i \quad (\text{Eq. 23})$$

$$\sigma^2 = \sum_{i=1}^N (i - \mu)^2 S_i \quad (\text{Eq. 24})$$

The steady-state probabilities results are shown for two SNR cases with  $N=64$  in **Figure 13**. The tracking error standard deviation for the SNR = -2dB case is 14.7 degrees rms whereas it is 9.9 degrees rms for the SNR = +2dB case (**Figure 14**).

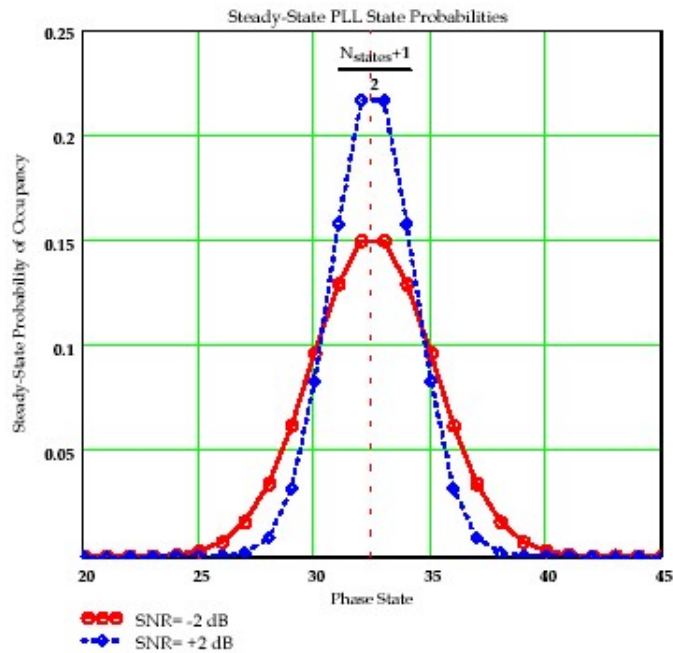


Figure 13: Tracking error standard deviation (in degrees rms) and effective loop SNR (dB) versus input SNR (dB).

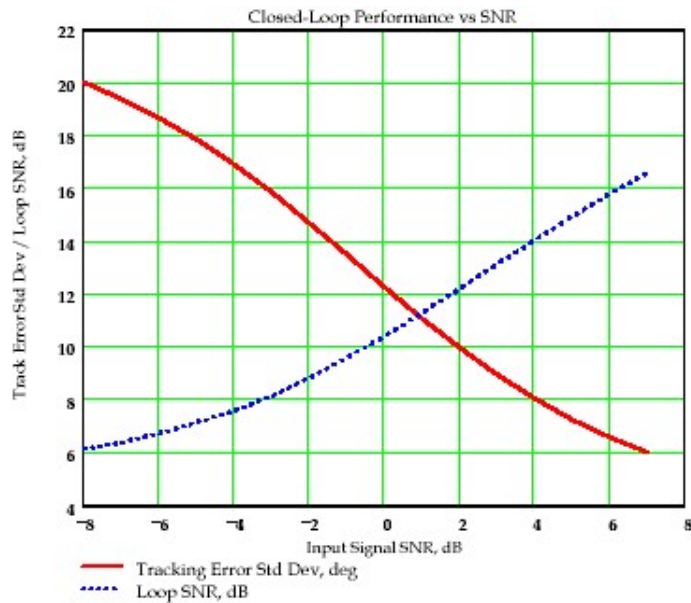


Figure 14: Steady-state probabilities).

Another important quantity related to low SNR PLL operation is the quantity known as "mean-time to cycle-slip". This can be directly computed from the transition probabilities in a similar fashion as described in References 13 and 14.

**Minimum Variance Estimator**

The design of a near-optimal PLL can be investigated by considering the phase-tracking problem as a minimum-variance estimation problem. Assume that we have a received signal that is represented by:

$$r(t) = s(t) + n(t) \quad (Eq. 25)$$

in which  $n(t)$  represents complex Gaussian channel noise and  $s(t)$  represents a complex sinusoid as

$$s(t) = A \exp[-j\omega_p t - j\theta] \quad (Eq. 18)$$

If the received signal is discretized in time ( $t_k = kT_s$ ), noise samples at  $t_k$  are assumed to be

uncorrelated, and the estimates for the sinusoid's parameters are given by  $\hat{A}$ ,  $\hat{\omega}$  and  $\hat{\theta}$ , the variance for the joint estimate is given by:

$$\sigma^2 = \sum_k \left| r(t_k) - \hat{A} \exp(-j\hat{\omega}t_k - j\hat{\theta}) \right|^2 \quad (Eq. 27)$$

This can be expanded as:

$$\sigma^2 = \sum_k \left[ \hat{A}^2 + |r(t_k)|^2 - 2\hat{A} \text{Re} \left\{ r(t_k) \exp(j\hat{\omega}t_k + j\hat{\theta}) \right\} \right] \quad (Eq. 28)$$

Assuming that the PLL has already achieved frequency-lock, we will assume that  $\hat{\omega} = \omega_o$  and there is no frequency error present. Minimizing the estimator variance with respect to each individual parameter separately results in the following partial derivatives:

$$\frac{\partial \sigma^2}{\partial \hat{A}} = 2K\hat{A} - 2 \sum_k \text{Re} \left\{ r(kT) \exp(j\omega_o kT + j\hat{\theta}) \right\} \quad (Eq. 29)$$

$$\frac{\partial \sigma^2}{\partial \hat{\theta}} = 2\hat{A} \sum_k \text{Im} \left[ r_k \exp(j\omega_o kT_s + j\hat{\theta}) \right] \quad (Eq. 30)$$

where  $\hat{A}$  is always a real quantity. The estimators that minimize the tracking error variance are then given as:

$$\sum_k \text{Im} \left[ r_k z_k \exp(j\hat{\theta}) \right] = 0 \quad (Eq. 31)$$

$$\hat{A} = \frac{1}{K} \sum_k \text{Re} \left[ r_k z_k \exp(j\hat{\theta}) \right] \quad (Eq. 32)$$

in which K is the total number of signal samples involved and  $z_k = \exp(j\omega T_s)$ . Although the estimator for  $\hat{A}$  involves first knowing  $\hat{\theta}$ , no prerequisite knowledge of  $\hat{A}$  is explicitly required in Equation 31 in order to find the best phase estimate. The implementation structure suggested by Equation 31 for the minimum-variance phase estimator is shown in **Figure 15**.<sup>19</sup>

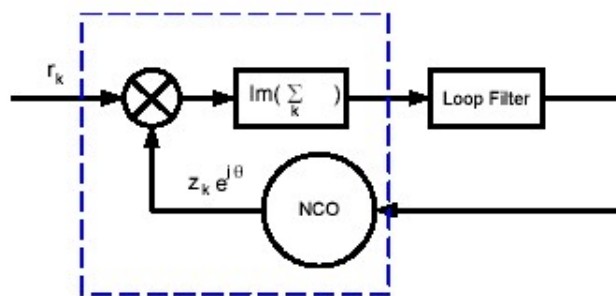


Figure 15: Minimum-variance estimator cast as a PLL.

### Maximum-Likelihood Estimator

Another estimator form can be derived based upon maximizing probability or what is called "likelihood" in estimation theory. In the case of a real sinusoid of unknown phase in real additive Gaussian noise similar to the situation we just examined, we seek to pick an estimate for  $\theta$  that maximizes the probability:

$$P(\underline{r}) = (2\pi)^{-\frac{K}{2}} |R|^{-\frac{1}{2}} \exp \left\{ -\frac{1}{2} [\underline{r} - \underline{s}]^T R^{-1} [\underline{r} - \underline{s}] \right\}$$

where  $\underline{r}$  and  $\underline{s}$  represent the K-dimensional measurement and signal estimate, and R is the KxK

correlation matrix. In this real case being considered,  $s_k = A \cos(\omega_0 k T_s + \theta)$ . We can equivalently seek to maximize the log-likelihood function of  $\theta$  which is given by:

$$L(\theta) = -\frac{K}{2} \log(2\pi) - \frac{1}{2} \log(|R|) - \frac{1}{2} [(r - \underline{s})^T R^{-1} (r - \underline{s})] \quad (\text{Eq. 34})$$

Assuming that the noise samples have equal variances and are uncorrelated,  $R = \sigma_n^2 I$ , where  $I$  is the  $K \times K$  identity matrix. In order to maximize Equation 34 with respect to  $\theta$ , a necessary condition is that the derivative of Equation 34 with respect to  $\theta$  be zero, or equivalently:

$$\begin{aligned} \frac{\partial L}{\partial \theta} &= \frac{\partial}{\partial \theta} \sum_k [r_k - A \cos(\omega_0 t_k + \theta)]^2 = 0 \\ &= \sum_k 2[r_k - A \cos(\omega_0 t_k + \theta)] A \sin(\omega_0 t_k + \theta) = 0 \quad (\text{Eq. 35}) \end{aligned}$$

Simplifying this result further and discarding the double-frequency terms that results, the maximum-likelihood estimate for  $\theta$  is that value that satisfies the constraint:

$$\overline{\sum_k r_k \sin(\omega_0 t_k + \hat{\theta})} = 0 \quad (\text{Eq. 36})$$

The top-line indicates that double-frequency terms are to be filtered out and discarded. This result is equivalent to the minimum-variance estimator derived earlier in Equation 31.

## Wrap Up

Diverse design perspectives can be utilized to improve and extend our basic understanding of the PLL concept. Mathcad worksheets for most of the results presented in this paper can be found at :

[http://www.siliconrfsystems.com/design\\_notes.htm](http://www.siliconrfsystems.com/design_notes.htm).

In [Part 2](#) of this article, we will close out the theoretical discussions by looking at (i) the maximum a posteriori (MAP) estimator PLL form, (ii) the Cramer-Rao bound which provides helpful insights into achievable theoretical performance, and finally (iii) the PLL derived based upon Kalman filtering concepts. The balance of the article will look at several real-world applications using the PLL concept.

**Editor's Note:** To view [Part 2](#), [click here](#).

## References

1. de Bellescize, H., "La Reception Synchrone," *Onde Electr*, Vol. 11, June 1932, pp. 230-240.
2. Sepe, R.B., R.I. Johnston, "Frequency Multiplier and Frequency Waveform Generator," U.S. Patent No. 3,551,826, December 29, 1970.
3. Crawford, J.A., *Frequency Synthesizer Design Handbook*, Artech House, 1994. Gardner, F.M., *Phaselock Techniques, 2nd Ed.*, John Wiley & Sons, 1979.
4. Best, R.E., *Phase-Locked Loops Theory Design & Applications*, McGraw-Hill Book, 1984.
5. Adler, R., "A Study of Locking Phenomena in Oscillators," *Proc. IRE*, June 1946.
6. Kurokawa, K., "Injection Locking of Microwave Solid-State Oscillators," *Proc. IEEE*, Oct. 1973.
7. Dewan, E.M., "Harmonic Entrainment of van der Pol Oscillations: Phaselocking and Asynchronous Quenching," *IEEE Trans. Automatic Control*, Oct. 1972.
8. Uzunoglu, V., White, M.H., "Synchronous and the Coherent Phase-Locked Synchronous Oscillators: New Techniques in Synchronization and Tracking," *IEEE Trans. Cir. & Sys.*, July 1989.
9. Blanchard, A., *Phase-Locked Loops Application to Coherent Receiver Design*, John Wiley & Sons, 1976.
10. Van Trees, H., *Detection, Estimation and Modulation Theory, Part II*, John Wiley & Sons.
11. Egan, W.F., *Phase-Lock Basics*, John Wiley & Sons, 1998.
12. Holmes, J.K., *Coherent Spread Spectrum Systems*, John Wiley & Sons, 1982.
13. Holmes, J.K., "Performance of a First-Order Transition Sampling Digital Phase-Locked Loop Using Random-Walk Models," *IEEE Trans. Comm.*, April 1972.
14. Viterbi, A.J., *Principles of Coherent Communication*, McGraw-Hill.
15. Meyr, H., et al., *Digital Communication Receivers Synchronization, Channel Estimation, and Signal Processing*, John Wiley & Sons, 1998.
16. Srinath, M.D., Rajasekaran, P.K., *An Introduction to Statistical Signal Processing with Applications*, John Wiley & Sons, 1979.

17. Lindsey, W.C., Simon, M. K., *Telecommunication Systems Engineering*, Prentice-Hall, 1973.
18. Ziemer, R.E., Peterson, R.L., *Digital Communications and Spread Spectrum Systems*, Macmillan, 1985.
19. Scharf, L.L., *Statistical Signal Processing Detection, Estimation, and Time Series Analysis*, Addison-Wesley, 1991.

#### **About the Author**

**James Crawford** is the president/CEO and director of communication systems at Silicon RF Systems, Inc. Prior to this position, James served as the CTO of Magis Networks. He can be reached at [jcrawford@siliconrfsystems.com](mailto:jcrawford@siliconrfsystems.com).



[Copyright © 2003 CMP Media, LLC](#) | [Privacy Statement](#)



## CommsDesign

### Tutorial on PLLs: Part 2

James A. Crawford, Silicon RF Systems

" 06, 2004 (4:00 H)

URL: <http://www.commsdesign.com/showArticle.jhtml?articleID=19502356>

In [Part 1](#) of this article, we looked at a number of phase-locked loop (PLL) concepts ranging from continuous and sampled control systems to estimation theory based perspectives. Now, in Part 2, we will continue are examination of the PLL concept in the estimation theory sense by looking at maximum a posteriori (MAP)-based PLLs and the fundamental performance limits described by the Cramer-Rao bound. Our theoretic involvement will culminate with a Kalman filtering perspective for the PLL. The balance of this article will utilize the PLL concept in several real-world applications.

#### MAP-based Estimators

The MAP estimator form is used for the estimation of random parameters whereas the maximum-likelihood (ML) form is generally associated with the estimation of deterministic parameters. From Bayes Rule, we know that given an observation  $z$  that *Equation 1* is true.

Equation 1 below can be re-written in the logarithmic form as shown in *Equation 2* below.

This log probability may be maximized by setting the derivative with respect to  $\theta$  to zero thereby creating the necessary condition that is shown in *Equation 3* below.

If the density  $p(\theta)$  is not known, we are forced to ignore the second term in Equation 3, which leads naturally to the maximum-likelihood form as shown in *Equation 4* below.

Although the MAP and ML estimators are not the same in the strict sense, the MAP estimator takes on the form of the maximum-likelihood (ML) estimator in the absence of sufficient prior knowledge of  $\theta$ .

The similarities between the minimum mean-square error (MMSE), ML, and MAP estimators should not go unnoticed. In the Gaussian noise case, the observed signal is given by:

$$p(\theta|z) = \frac{p(z|\theta)p(\theta)}{p(z)} \quad (\text{Eq. 1})$$

$$\text{Ln}[p(\theta|z)] = \text{Ln}[p(z|\theta)] + \text{Ln}[p(\theta)] - \text{Ln}[p(z)] \quad (\text{Eq. 2})$$

$$\frac{d}{d\theta} \left\{ \text{Ln}[p(z|\theta)] + \text{Ln}[p(\theta)] \right\}_{\theta=\hat{\theta}_{\text{MAP}}} = 0 \quad (\text{Eq. 3})$$

$$\frac{d}{d\theta} \left\{ \text{Ln}[p(z|\theta)] \right\}_{\theta=\hat{\theta}_{\text{ML}}} = 0 \quad (\text{Eq. 4})$$

$$z(t) = y(t, \theta) + v(t) \quad \text{for } t_o \leq t \leq t_f \quad (\text{Eq. 5})$$

in which  $v(t)$  is the noise and  $\theta$  is the nonrandom parameter of interest, it can be shown that the ML estimate for  $\theta$  is given by:

$$\int_{t_o}^{t_f} [z(t) - y(t, \theta)] \frac{\partial y(t, \theta)}{\partial \theta} dt \Big|_{\theta=\hat{\theta}_{\text{ML}}} = 0 \quad (\text{Eq. 6})$$

In the jointly Gaussian case where  $\theta$  is assumed to be a random parameter having a variance of  $\sigma_\theta^2$ , use of Equation 3 leads to the result that:

$$\hat{\theta}_{MAP} = \frac{2}{N_o} \sigma_\theta^2 \int_{t_0}^{t_f} [z(t) - y(t, \theta)] \frac{\partial y(t, \theta)}{\partial \theta} dt \Big|_{\theta = \hat{\theta}_{MAP}} \quad (Eq. 7)$$

These two results illustrate how similar the ML and MAP estimates can appear. The Fundamental Theorem of Estimation Theory<sup>22</sup> states that the estimator that minimizes the mean-square error is given by:

$$\hat{\theta}_{opt} = \mathbb{E}[\theta | z] \quad (Eq. 8)$$

It can also be shown that the best linear unbiased estimator (BLUE) form takes on the form of the weighted least-squares estimator given that the proper sample weighting is applied.

In [Part 1](#) of this article, we found that the ML estimator for the signal phase utilized a gradient error metric that sought to drive any quadrature (or orthogonal) signal components to zero. This is not unlike the Orthogonality Principle in estimation theory, which stipulates that any residual estimation error should be orthogonal (i.e., uncorrelated) with the observations as:

$$\mathbb{E}[(\hat{\theta} - \theta)z] = 0 \quad (Eq. 9)$$

More information on the fundamentals of estimation theory can be found in References 20, 21, and 22.

### Performance Limits From the Cramer-Rao Bound

In the case of unbiased estimators for non-random parameters, the Cramer-Rao Bound (CRB) provides a lower bound for the estimation error variance achievable. One of the most important aspects of the CRB and bounds like it is that the difficulty of a given design objective can be very quickly judged by comparing a given requirement with the appropriate bound. In other words, it can be embarrassing to find out after already expending a great deal of time and effort on a problem that the requirement runs contrary to the laws of physics.

In the single-parameter case, the CRB is usually presented in two different equivalent forms as:<sup>20,21,22</sup>

$$\begin{aligned} \text{var}[(\hat{\theta} - \theta) | \theta] &= \mathbb{E}[(\hat{\theta} - \theta)^2 | \theta] \geq \left\{ \mathbb{E} \left[ \left[ \frac{\partial \ln p(z | \theta)}{\partial \theta} \right]^2 | \theta \right] \right\}^{-1} \\ \text{var}[(\hat{\theta} - \theta) | \theta] &\geq - \left\{ \mathbb{E} \left[ \frac{\partial^2 \ln p(z | \theta)}{\partial \theta^2} | \theta \right] \right\}^{-1} \end{aligned} \quad (Eq. 10)$$

When multiple parameters are being estimated (e.g., amplitude, phase, frequency), the CRB takes the form of the Fisher Information Matrix. The interested reader should consult References 19, 20, 21, and 22 for additional information on this topic.

It is of interest to compare the MAP and PLL phase estimators in terms of some performance measures. In order to do this, we first obtain the variance of each estimator. As developed in [Part 1](#), the steady-state first-order (and second-order) PLL phase estimator probability density is taken to be the Tikhonov probability density function that is given by:

$$p(\hat{\theta} - \theta) = \frac{\exp[\alpha \cos(\hat{\theta} - \theta)]}{2\pi I_0(\alpha)} \quad (Eq. 11)$$

where  $I_0()$  is the zeroth-order modified Bessel function of the first kind and  $\alpha$  is the SNR within the PLL. The variance for the PLL estimator is given by:<sup>13</sup>

$$\sigma_{PLL}^2 = \frac{\pi^2}{3} + 4 \sum_{n=1}^{\infty} \frac{(-1)^n I_n(\alpha)}{n^2 I_0(\alpha)} \quad (Eq. 12)$$

These results and the linear result in which  $\sigma_\theta^2 = \alpha^{-1}$  are plotted for comparison purposes in [Figure 1](#).



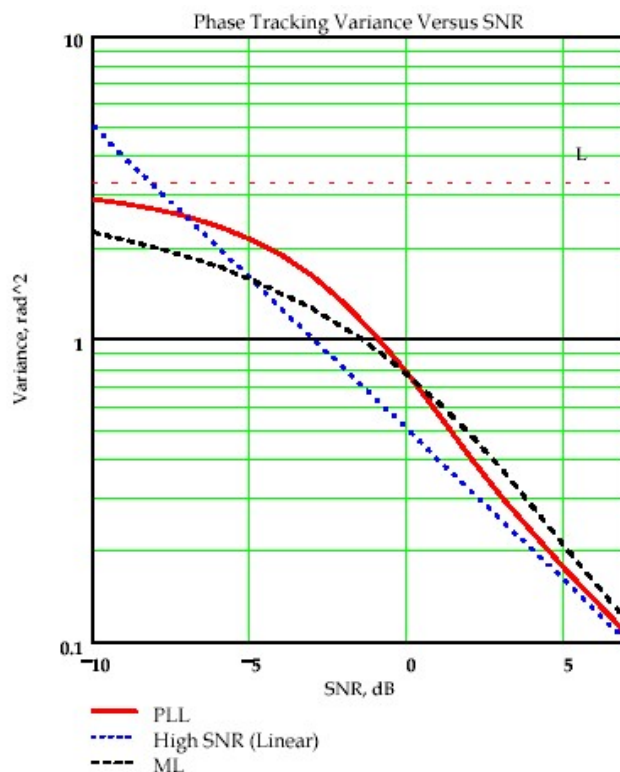


Figure 1: Tracking variance for MAP and PLL phase estimators versus SNR.

### Kalman Filtering

The PLL can be cast as an extended Kalman filter and hence it is an approximate solution for the optimal nonlinear filtering problem.<sup>9</sup> The Kalman filter is a set of mathematical equations that provides an efficient recursive means to estimate the state  $x$  of a process, in a way that minimizes the mean of the squared error. The filter is very powerful in several aspects: it supports estimation of past, present, and even future events.<sup>10</sup>

The Kalman filter addresses the general problem of trying to estimate the state  $x$  of a discrete-time controlled process that is governed by the linear stochastic difference equation of the form:

$$\underline{x}_{k+1} = A\underline{x}_k + B\underline{u}_k + \underline{w}_k \quad (\text{Eq. 13})$$

with measurements given by:

$$\underline{z}_{k+1} = H\underline{x}_{k+1} + \underline{v}_k \quad (\text{Eq. 14})$$

The  $A$ ,  $B$ , and  $H$  matrices can be time-variable but are shown here as constant. The random  $\underline{w}_k$  and  $\underline{v}_k$  represent the process and measurement noise respectively, and they are assumed to be statistically independent with covariance matrices  $Q$  and  $R$  respectively. Vector  $\underline{u}_k$  is the input to the system.

The mean-squared filtered estimate of the system state at time  $k+1$  is represented by  $\hat{\underline{x}}(k+1|k+1)$ , and it can be written in predictor-corrector form as shown in **Figure 2**.

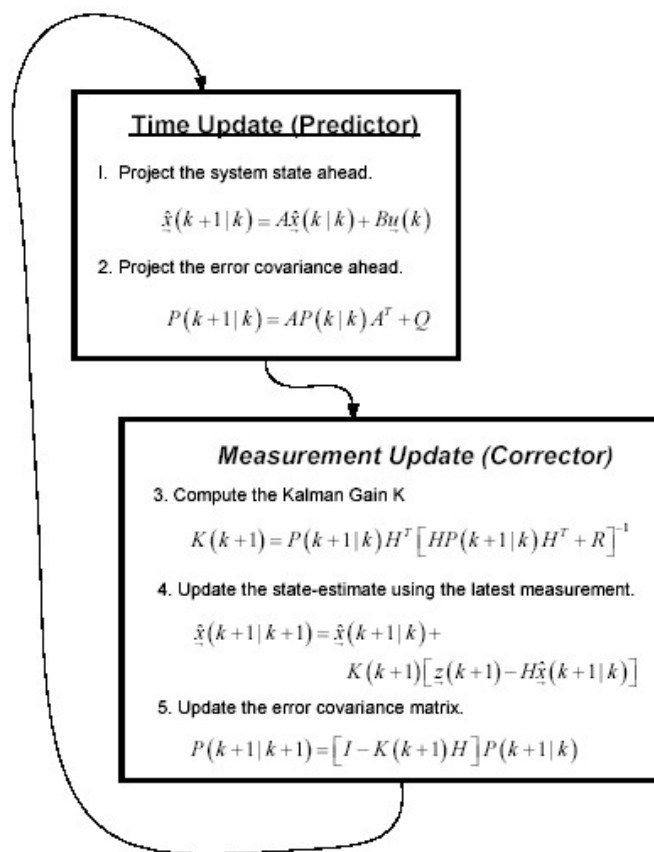


Figure 2: Organization of Kalman filter as a predictor-corrector sequence.<sup>10</sup>

The similarities of the Kalman filter with other time-stationary results are striking. In the case of the best linear unbiased estimate (BLUE), its recursive structure may be written in an almost identical form except that we have no time prediction steps since we have access to no system state information for the BLUE. Its formulation is shown in **Figure 3**.

**Best Linear Unbiased Estimate (BLUE)**

$$\hat{\theta}_{BLUE}(k+1) = \hat{\theta}_{BLUE}(k) + K_{BLUE}(k+1)[z(k+1) - H\hat{\theta}_{BLUE}(k)]$$

$$K_{BLUE}(k+1) = P(k+1)HR^{-1}$$

$$P^{-1}(k+1) = P^{-1}(k) + H^T R^{-1}H$$

Figure 3: Recursive equation formulation for BLUE.

The recursive Kalman equations lend themselves very easily to implementation within a second-order digital phase-locked loop (DPLL). This has been done before in References 11 and 12.

Although the Kalman filter requires current information about the noise covariance in its execution through the Q and R matrices, it is particularly adept at improving the tracking performance in situations which are not time-stationary. As the structure content of the signal being tracked increases, the Kalman filter can deliver substantial performance gains over other methods that do not exploit state estimation.

## PLL Applications

### 1. RF Frequency Synthesis Using Charge-Pump Based PLLs

The National Semiconductor line of Platinum frequency synthesizer devices revolutionized the world of frequency synthesis in the early 1990's by delivering unprecedented predictably-reliable phase noise performance in a highly-integrated low-cost device. These devices had a host of very nice features about them, but most notable was the low phase noise performance of the charge-pump phase detector along with the very low reference spur levels achievable. The excellent balance and leakage characteristics of the phase detector made it possible to implement a complete PLL with a very modest loop filter.

#### 1. Classic Type-2 Charge-Pump Implementation

The circuit schematic for the classic type-2 fourth-order PLL is shown here in **Figure 4**. The current noise sources associated with each resistor are shown shunted across each respective resistor, and the reference-related and voltage-controlled oscillator (VCO) self-noise make up the remainder of the major noise contributors.

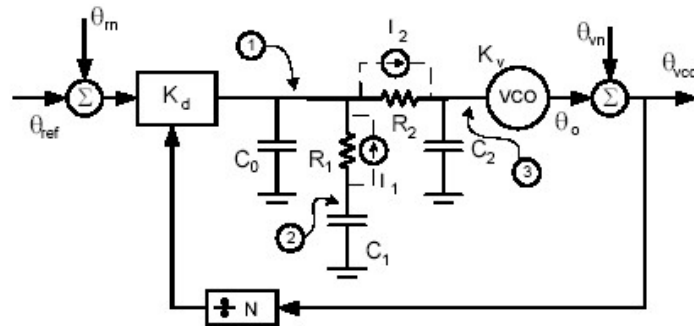


Figure 4: Circuit Diagram for type-2 fourth-order PLL using charge-pump phase detector.

The normal approach that is taken to analyze this kind of system is to solve the nodal equations for the appropriate transfer functions algebraically.<sup>4</sup> A streamlined approach is taken here where the same nodal equations are used but the customary algebraic manipulations are avoided by using matrix methods. The matrix equation that describes the circuit in Figure 4 can be quickly written down in Laplace transform form as:

$$\begin{bmatrix} sC_0 + G_1 + G_2 & -G_1 & -G_2 & \frac{K_d}{N} \\ -G_1 & sC_1 + G_1 & 0 & 0 \\ -G_2 & 0 & G_2 + sC_2 & 0 \\ 0 & 0 & -\frac{K_v}{s} & 1 \end{bmatrix} \begin{bmatrix} V_1 \\ V_2 \\ V_3 \\ \theta_{VCO} \end{bmatrix} = \begin{bmatrix} I_1 - I_2 + K_d \theta_m \\ -I_1 \\ I_2 \\ \theta_m \end{bmatrix} \quad (\text{Eq. 15})$$

where  $G_i = (R_i)^{-1}$  and the  $I_j$  represent the Johnson current noise sources associated with each resistor. Analysis tools like Matlab and Mathcad can be used to numerically solve this equation for the transfer functions of interest and for closed-loop noise performance quantities. The noise current for the  $j^{\text{th}}$  resistor is given as:

$$I_j = \sqrt{\frac{4kT_e}{R_j}} \quad (\text{Eq. 16})$$

and all of the noise sources are assumed to be statistically independent.

The phase detector referenced phase noise floor for the National Semiconductor Platinum series devices is given by:

$$L_{PD} = L_{Floor} + 20 \text{Log}_{10}(F_{VCO}) - 10 \text{Log}_{10}(F_{REF}) \quad (\text{Eq. 17})$$

where  $L_{Floor} = -205/-210/-211/-218$  dBc/Hz for the LMX2315/LMX2306/LMX2330/LMX2346 devices respectively. This model or another can be used for the reference noise level represented in Equation 15 by  $\theta_{rn}$ . Leeson's model can be similarly used for the VCO self-noise term represented by  $\theta_{vn}$  in Equation 15, recognizing that this noise contribution is frequency-dependent as given by:

$$L_{VCO}(f) = 10 \text{Log}_{10} \left[ \frac{FkT_e}{2P_o} \left( 1 + \left( \frac{F_c}{2Q_L f} \right)^2 \right) \right] \quad (\text{Eq. 18})$$

in which  $F$  is noise factor,  $k$  is the Boltzmann's constant,  $T_0 = 290$  degrees Kelvin,  $P_0$  is the power extracted from the actual resonator in Watts,  $F_c$  is the VCO center frequency in Hz, and  $Q_L$  is the loaded resonator Q-factor. Additional terms are often added within the parenthesis to account for  $1/f$  noise, etc., but these rarely survive the closed-loop action of the PLL and have consequently not been included here.

The transient response of the PLL to a step-change in phase or frequency can be similarly computed using numerical techniques. The approach taken here is to substitute the Laplace transform of a step-frequency error given by  $2\pi\Delta F/s^2$  in for  $\theta_{vn}$  in Equation 15, and then compute the Fourier transform for  $\theta_{VCO}$  at an equally-spaced grid of frequencies from which the inverse FFT provides the time-domain response. An example time-domain response is shown in **Figure 5**. The ensuing details for both of these example results have purposely been omitted for brevity whereas they can be found online.<sup>6</sup>

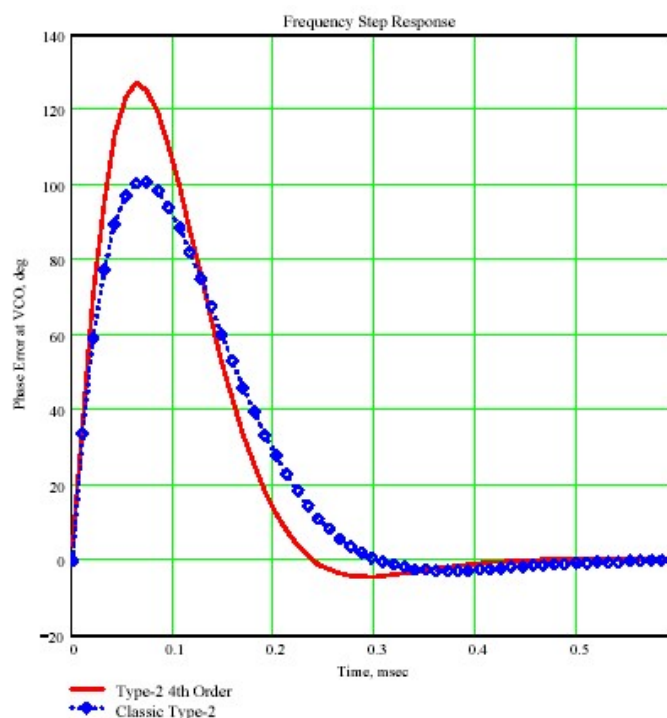


Figure 6: Example time-domain response to step-frequency change using FFTs.

Several design procedures are available for designing "optimal" PLL loop filters. Whenever the word optimal is used however, designers should ask the question, "Optimal with respect to what criteria?"

Some communication systems are primarily concerned with frequency error whereas others are concerned with phase error. If the wrong criteria is adopted, the design can often result in being more difficult than necessary. It is therefore very attractive to have an interactive tool that permits a simultaneous examination of both the time as well as output spectrum domains.

### Phase Noise Impact on Communication Systems

Phase noise manifests itself in primarily two undesired phenomenon when it comes to wireless communications and frequency synthesis. Close-in<sup>1</sup> phase noise interferes with coherence in the receiver and in the case of QAM signal constellation, causes adjacent constellation points to be received more likely in error when channel noise is present. (Amplitude noise at the output of a properly designed synthesizer should be 20 dB or more below the phase noise level, and is therefore rarely a consideration.)

In frequency-modulated systems, phase noise can be equivalently expressed as a residual FM noise and it similarly adds to confusion in the receiver as to which frequency was truly sent by the transmitter. Far-out phase noise degrades channel selectivity, adjacent channel occupancy, and receiver third-order intercept point due to reciprocal mixing. Only a few of the most common digital communication waveforms will be considered here due to space limitations.

The close-in phase noise impairment to (uncoded) bit error rate performance is most often computed using the Tikhonov probability distribution function for the noise. For large signal-to-noise ratio (SNR) arguments, numerical evaluation of the zeroth-order Bessel function can become problematic and it is more convenient to closely approximate this density function as:

$$p_{\theta}(\theta, \sigma_{\theta}^2) = \sqrt{\frac{1}{2\pi\sigma_{\theta}^2}} \exp\left[-\frac{\cos(\theta)-1}{\sigma_{\theta}^2}\right] \quad (\text{Eq.19})$$

in which  $\sigma_{\theta}^2$  is the variance of the phase noise process involved. This variance is normally calculated as:

$$\sigma_{\theta}^2 = 2 \int_{F_L}^{F_S} L(f) df \quad (\text{Eq.20})$$

where  $L(f)$  is the phase noise power spectral density of the local oscillators involved in  $\text{rad}^2/\text{Hz}$ ,  $F_S$  is the symbol rate, and  $F_L$  is a lower frequency limit normally given as  $0.01 F_S$  or thereabouts, depending upon the carrier-recovery baseband processing that may be present in the complete system. These definitions apply for a single-carrier system but need some additional enlargement in the case of multi-carrier systems like orthogonal frequency division multiplexing (OFDM). In the case of QAM-style digital modulations, the (uncoded) symbol error rate can then be computed as:

$$P_{SER} \left( \frac{E_s}{N_o}, \sigma_\theta \right) = \int_{-\pi}^{+\pi} P_s \left( \frac{E_s}{N_o} | \theta \right) p(\theta, \sigma_\theta^2) d\theta \quad (Eq. 21)$$

Some results computed in this manner may be found in Reference 8. The conditional symbol-error-rate formulas for coherent binary phase-shift keying (BPSK) and quadrature PSK (QPSK) performance are respectively given as:

$$P_{SER\_BPSK} \left( \frac{E_b}{N_o} | \theta \right) = \frac{1}{2} \operatorname{erfc} \left[ \sqrt{\frac{E_b}{N_o}} \cos(\theta) \right] \quad (Eq. 22)$$

$$P_{SER\_QPSK} \left( \frac{E_b}{N_o} | \theta \right) = \frac{1}{4} \operatorname{erfc} \left\{ \sqrt{\frac{E_b}{N_o}} [\cos(\theta) - \sin(\theta)] \right\} + \frac{1}{4} \operatorname{erfc} \left\{ \sqrt{\frac{E_b}{N_o}} [\cos(\theta) + \sin(\theta)] \right\} \quad (Eq. 23)$$

The conditional symbol error rate relationships for other square-QAM signal constellations like 64-QAM can be found in Reference 7.

It should come as no surprise that BPSK shows little susceptibility to phase noise related performance loss as shown in **Table 1** since it is essentially an amplitude-based modulation type. Performance degrades significantly as the signal constellation size increases, culminating in sub-one degree rms phase noise being desirable for 64-QAM in order to avoid appreciable  $E_b/N_o$  loss.

**Table 1: QAM Uncoded Symbol Error Rate with Phase Noise**

[Click here for table 1](#)

In the case of carrier-recovery in which coherent demodulation is to be performed on QAM-type signals, the Costas loop has found wide-spread use as an unbiased low-variance practical solution. It can be shown that the Costas loops for BPSK and QPSK are equivalent to 2nd and 4th power non-linearities followed by a PLL. Block diagrams for the BPSK and QPSK Costas loops are shown in **Figure 6** and **Figure 7** respectively.

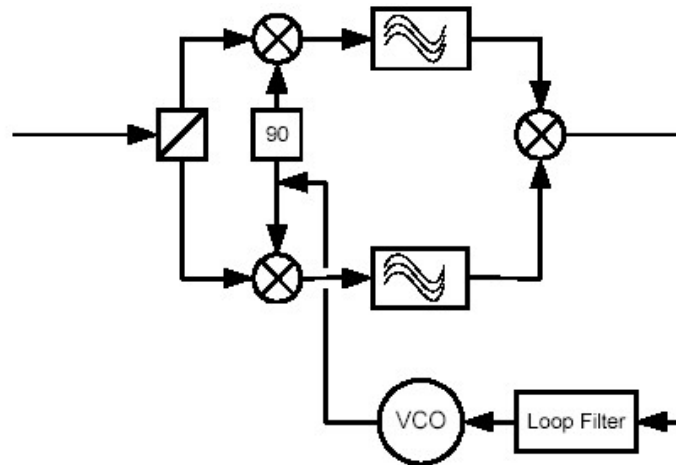


Figure 6: MAP-based Costas carrier recovery PLL for BPSK.<sup>14</sup>

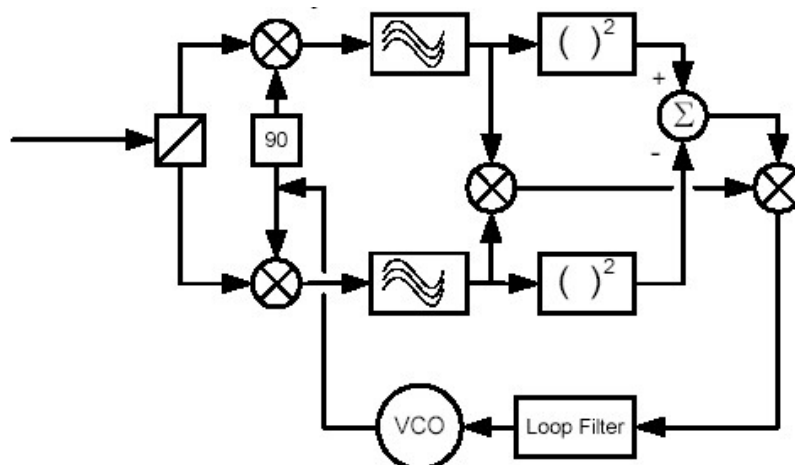


Figure 7: MAP-based carrier recovery PLL for QPSK.<sup>15</sup>

### Symbol Timing Recovery

Symbol timing recovery is required in both wired as well as wireless systems and quite often employs PLL-like circuitry or algorithms. Timing errors in this process lead to (i) a loss associated with missing the correlation peak from the receive matched filter as well as (ii) additional inter-symbol interference (ISI) from time-adjacent data symbols. In order to properly design the time tracking loop, we must first know the conditional error probability associated with a static timing error so that it can be used in a manner very similar to that used in Equation 21.

In the example that we will consider, the transmit pulse shape is assumed to be a square-root raised-cosine pulse having an excess bandwidth parameter  $\alpha$  of 0.50. The filter bandwidth time symbol time duration quantity for other filters used in this paper is referred to as BT. The Fourier transform for such a pulse is given by:

$$S(f) = \begin{cases} \sqrt{T_{\text{sym}}} & 0 \leq |f| \leq \frac{1-\alpha}{2T_{\text{sym}}} \\ \sqrt{\frac{T_{\text{sym}}}{2} \left[ 1 - \sin \left( \frac{\pi T_{\text{sym}}}{\alpha} \left( f - \frac{1}{2T_{\text{sym}}} \right) \right) \right]} & \frac{1-\alpha}{2T_{\text{sym}}} \leq |f| \leq \frac{1+\alpha}{2T_{\text{sym}}} \end{cases} \quad (\text{Eq. 24})$$

The receiver is assumed to use a continuous-time  $N=3$  Butterworth filter as a close approximation for the ideal matched filter and its Fourier transform may be written as:

$$H_{\text{rx}}(s) = \frac{1}{\left(\frac{s}{\omega_c}\right)^3 + 2\left(\frac{s}{\omega_c}\right)^2 + 2\left(\frac{s}{\omega_c}\right) + 1} \quad (\text{Eq. 25})$$

where  $\omega_c$  is the -3 dB corner frequency in rad/sec. In the absence of noise, the individual pulse shape observed at the output of  $H_{\text{rx}}(\ )$  may be directly computed by multiplying Equations 23 and 24 together in the frequency domain and performing an inverse FFT.

In the case where  $H_{\text{rx}}$  has  $BT = 0.50$ , this pulse shape is shown in **Figure 8**. In the absence of any timing error, the desired signal sample occurs coincident with the peak of the pulse as shown in Figure 8. ISI is clearly present as shown however, because sample values at time instants offset by  $\pm kT_{\text{sym}}$  are not all zero ( $k = \text{nonzero integer}$ ). For random data, these nonzero adjacent symbol samples create data-dependent noise at the receiver's decision making hardware thereby reducing the signal eye-opening thereby degrading system performance.

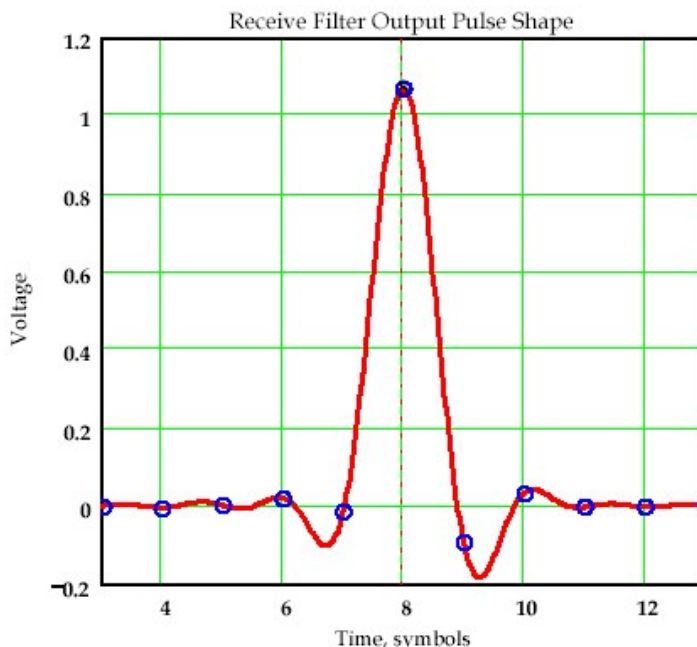


Figure 8: Individual pulse shape at receive filter output.

Insight into the ISI matter can be had by considering all possible sequences of four-symbol sequences possible and the eye diagram that is observed at the receive filter output. Eye diagrams for the  $\alpha = 0.50$  and  $0.40$  cases are shown in **Figures 9** and **10** respectively. The ISI and eye-closure are substantially worse for the  $\alpha = 0.40$  case as shown.

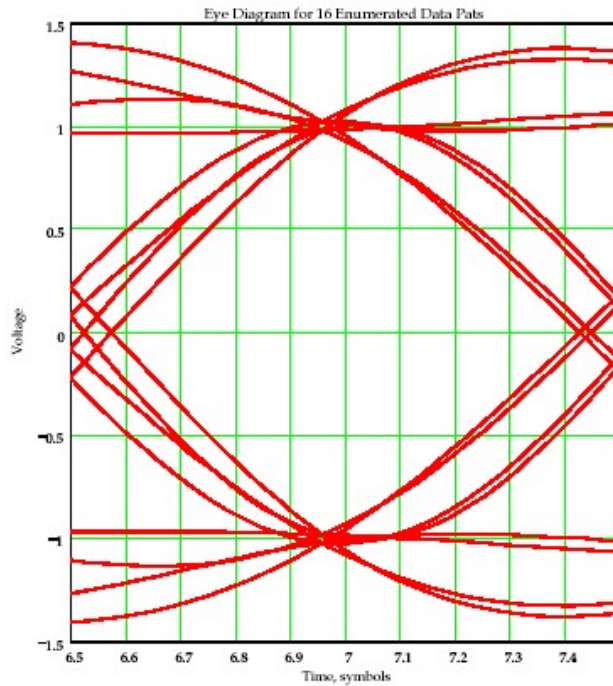


Figure 9: ISI pattern for 16 possible four-symbol sequences with excess bandwidth parameter = 0.50.

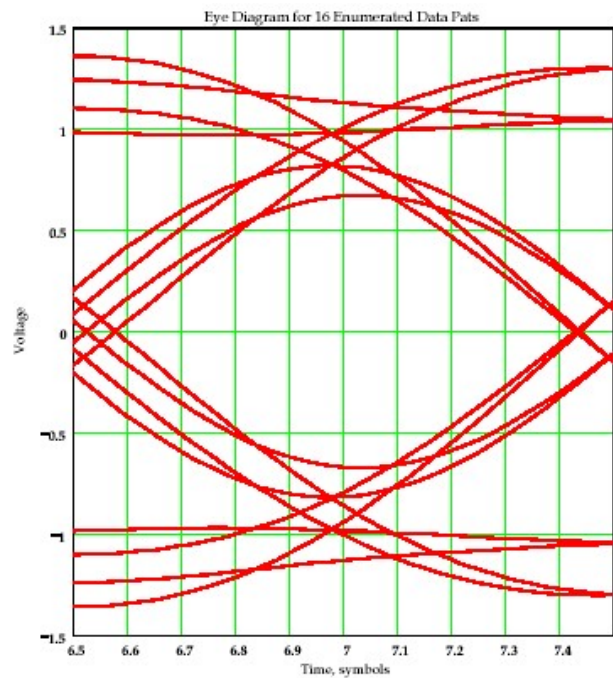


Figure 10: ISI pattern for 16 possible four-symbol sequences with excess bandwidth parameter = 0.40.

The symbol error rate for random +/-1 data can be mathematically computed by recognizing that the decision statistic consists of three components: (1) the desired signal, (2) additive Gaussian noise, and (3) data pattern-dependent ISI. Characteristic function methods may be used to combine the effects of the ISI and Gaussian noise as described in Reference 16 leading to the symbol error rate expression with static timing error  $\tau_e$  being given as:

$$P_e(\tau_e, \sigma) = \frac{1}{2} - \frac{1}{\pi} \int_0^{\infty} \frac{\sin[\omega r(\tau_e)]}{\omega} C(\omega, \tau_e) \exp\left(-\frac{1}{2} \sigma^2 \omega^2\right) d\omega \quad (Eq. 26)$$

where  $r(t)$  is the noise-free single-pulse shape at the receive filter output,  $\sigma^2$  is the variance of the Gaussian noise at the receive filter output, and  $C(\omega)$  is the characteristic function of the ISI noise. This can be shown to be given by:

$$C(\omega, \tau_e) = \prod_{\substack{m=-L \\ m \neq 0}}^L \cos[\omega r(\tau_e + mT_{sym})] \quad (Eq. 27)$$

The variance quantity specified in Equation 26 can be found from the equivalent noise bandwidth of the receive filter as:

$$\sigma^2 = \frac{N_0}{2} \int_{-\infty}^{+\infty} |H_{rx}(j\omega)|^2 d\omega \quad (\text{Eq. 28})$$

where  $N_0$  is the one-sided Gaussian white noise power spectral density.

The foregoing results were used to compute the effect of timing error on symbol error rate performance as a function of the receive filter product as shown in **Figure 11**. The optimal value for best performance is  $BT = 0.50$  which leads to a performance loss of only about 0.25 dB at an input  $E_s/N_0$  value of 9.6 dB which is quite remarkable.

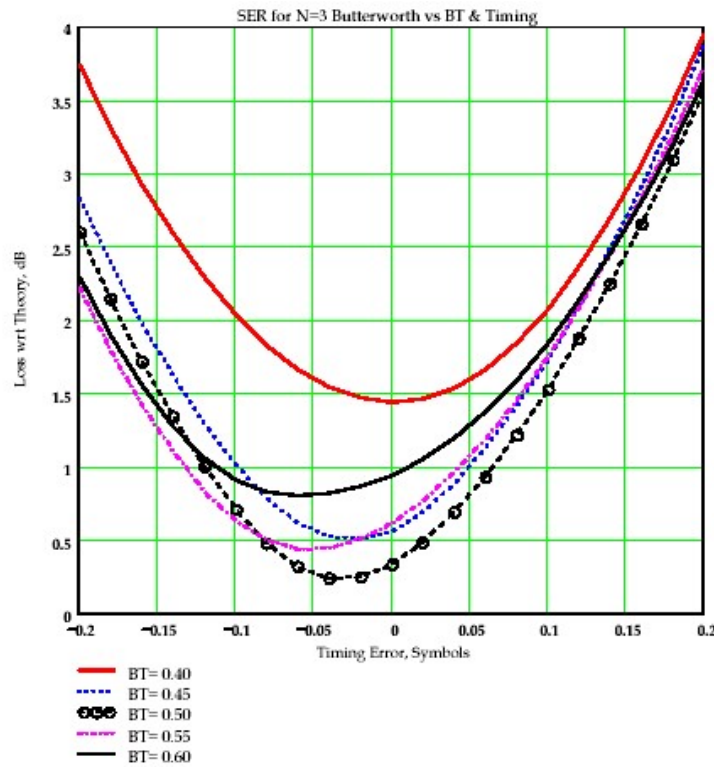


Figure 11: Symbol error rate versus static timing error and filter BT product.

The curves shown in Figure 11 can indirectly provide the needed conditional error probability like that used in Equation 21 thereby allowing the complete impact of imperfect PLL time-tracking behavior to be assessed.

In the context of hardware-based symbol timing recovery, many different types of timing error metrics are available, but one stands out in particular for very high-speed data applications in which most other detectors fall prey to meta-stability problems. This detector type was first patented by Hogge<sup>18</sup> and is shown here in **Figure 12**. This detector is rather uniquely equipped for extremely high-speed data applications and in this figure, is shown being used within a type-2 third-order PLL structure.



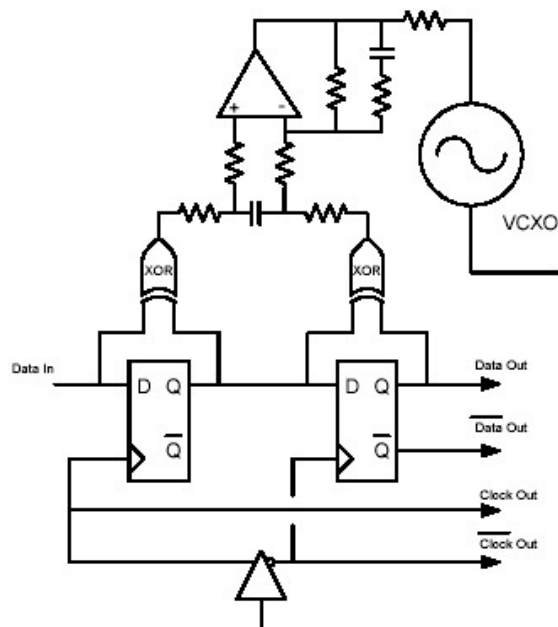


Figure 12: Hogge clock-recovery circuit within PLL structure.

### Wrap Up

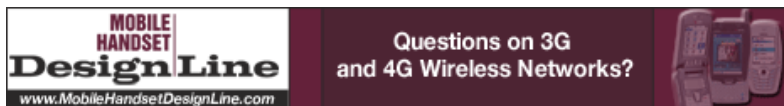
This two-part article has covered a wide range of PLL-related topics, but nonetheless space limitations precluded even mentioning other PLL-workhorses like Costas loops, joint timing and phase recovery PLLs, etc. If these articles succeeded in illustrating the versatile and pervasive aspects of the PLL concept, make a point in becoming more studious in PLLs. You will be glad that you did. **Editor's note:** To view Part 1, [click here](#).

### References

1. J.A. Crawford, *Frequency Synthesizer Design Handbook*, Artech House, 1994
2. J.A. Crawford, "Thoughts on Charge-Pump Phase Noise", 1999, (<http://www.siliconrfsystems.com/Papers/ChargePump.pdf>).
3. D. Banerjee, "PLL Performance", National Semiconductor
4. D. Banerjee, "PLL Performance, Simulation & Design", 3rd Ed., 2003, National Semiconductor, (<http://www.national.com/appinfo/wireless/files/Deansbook3.pdf>).
5. W.P. Robins, *Phase Noise in Signal Sources*, Peter Peregrinus Ltd., 1982.
6. J.A. Crawford, "U10650 Type-2 4th-Order PLL Worksheet", 24 March 2004.
7. J.A. Crawford, "Phase Noise Effects on Square-QAM Symbol Error Rate Performance, 2004, <http://www.siliconrfsystems.com/Papers/Phase%20Noise%20Effects%20on%20Square%20QAM%20v1.pdf>.
8. R. Gilmore, "Specifying Local Oscillator Phase Noise Performance- How Good is Good Enough?", <http://www.siliconrfsystems.com/Papers/U10236%20Phase%20Noise-%20How%20Good-%20Gilmore.pdf>.
9. P.O. Amblard et al., "Phase Tracking: What Do We Gain from Optimality? Particle Filtering Versus Phase-Locked Loops", March 2001.
10. G. Welch, G. Bishop, "An Introduction to the Kalman Filter", March 1, 2004.
11. P.F. Driessen, "DPLL Bit Synchronizer with Rapid Acquisition Using Adaptive Kalman Filtering Techniques", IEEE Trans. Comm. Sept., 1994.
12. A. Patapoutian, "On Phase-Locked Loops and Kalman Filters", IEEE Trans. Comm., May, 1999.
13. J.S. Lee, J.H. Huhgen, "An Optimum Phase Synchronizer in a Partially Coherent Receiver", IEEE Trans. Aerospace and Electronic Systems, July, 1971.
14. R.E. Ziemer, R.L. Peterson, *Digital Communications and Spread Spectrum Systems*, Macmillan, 1985.
15. J.A. Bingham, *The Theory and Practice of Modem Design*, John Wiley & Sons, 1988.
16. Ho, "Evaluation of Error Probability Including Intersymbol Interference", Bell System Technical Journal, Nov. 1970.
17. J.A. Crawford, "U10651 SER with Timing Error", March 2004.
18. C.R. Hogge, "A Self-Correcting Clock Recovery Circuit", IEEE Trans. Electronic Devices, December 1985.
19. H. Meyr, M. Moeneclaey, S.A. Fechtel, *Digital Communication Receivers Synchronization, Channel Estimation, and Signal Processing*, John Wiley & Sons, 1998.
20. M.D. Srinath, P.K. Rajasekaran, *An Introduction to Statistical Signal Processing with Applications*, John Wiley & Sons, 1979.
21. H.L. Van Trees, *Detection, Estimation, and Modulation Theory*, John Wiley & Sons, 1968.
22. J.M. Mendel, *Lessons in Theory for Signal Processing, Communications, and Control*, Prentice-Hall, 1995.
23. A. Gelb, *Applied Optimal Estimation*, The Analytical Sciences Corporation, 1996.

### About the Author

**James Crawford** is the president/CEO and director of communication systems at Silicon RF Systems, Inc. Prior to this position, James served as the CTO of Magis Networks. He can be reached at [jcrawford@siliconrfsystems.com](mailto:jcrawford@siliconrfsystems.com).



[Copyright © 2003 CMP Media, LLC](#) | [Privacy Statement](#)